Scannable Leaky-Wave Antenna Based on Ferrite-Blade Waveguide Operated Below the Cutoff Frequency

Morteza Mohammadi Shirkolaei [1] and Javad Ghalibafan [2]

[1]Department of Electrical Engineering, Shahid Sattari Aeronautical University of Science and Technology, Tehran 13846-63113, Iran

[2]Faculty of Electrical Engineering and Robotic, Shahrood University of Technology, Shahrood 3619995161, Iran

This article proposes a scannable leaky-wave antenna (LWA). The antenna consists of a ferrite-blade waveguide with a longitudinal slot on the upper wall, which has a tunable composite right-/left-handed (CRLH) property. The left-handed (LH) behavior of this structure is based on the negative effective permeability of the ferrite material and the negative effective permittivity of the waveguide excited below its cutoff frequency. First, based on the modal analysis and calculated dispersion relation, the unbalanced CRLH response of the ferrite-blade waveguide is investigated. Second, an LWA is presented by using a longitudinal slot on the upper wall of the proposed ferrite-blade waveguide, where the tunable balance CRLH response is achieved and analyzed by the transverse resonance method (TRM). The proposed LWA can provide backward, broadside, and forward radiations by a change in the operation frequency or the magnetic bias, independently. The given results show a $+59^\circ$ to -57° sweep in the radiation beam when the magnetic bias of the ferrite changed from 1400 to 1600 Oe at the sampling frequency of 6.4 GHz. Moreover, the results show that the frequency tuning range is more than 600 MHz (6.2–6.8 GHz). The peak gain and efficiency of the proposed antenna are 7.1 dBi and 78.5% at 6.6 GHz, respectively.

***Index Terms*— Composite right-/left-handed (CRLH), ferrite-blade waveguide, leaky-wave antenna (LWA), transverse resonance method (TRM).**

I. Introduction

RECENTLY, the composite right-/left-handed (CRLH) transmission lines as double negative metamaterials have been widely attractive in physic and engineering due to special inherent properties such as the negative refractive index and the reverse Doppler effect [1]–[8]. Generally, CRLHs can be classified into individual groups of balanced and unbalanced responses. In the unbalanced CRLH transmission line, the left-handed (LH) and right-handed (RH) regions are separated by a non-propagation frequency band. In contrast, the balanced CRLH response does not have any bandgap. The LH and RH frequency regions in the balanced case are connected at the transition frequency where the phase constant is 0. The balanced CRLH transmission lines have many applications in microwave devices and leaky-wave antenna (LWA) [9]–[11]. The LWA based on the balanced CRLH due to having a negative phase constant in the LH region, 0 in the transition frequency, and positive amount in the RH region, provide continuous beam scanning from backfire-to-endfire full space [12]–[15].

The conventional CRLH transmission lines are the cellular resonant structures consisting of a series capacitor and parallel inductors such as interdigital capacitors, transverse slots, shorted stubs, and split ring resonators (SRRs) [16]–[20]. However, these CRLH structures suffer from low-frequency bandwidth. To solve this problem, the tunable CRLH structures have been proposed in some previous works. For example, the varactors and p-i-n diodes have been used in [21] and [22]. However, the electrical dc bias lines limit the use of this CRLH structure in radiation applications.

The inherent negative effective permeability of the magnetized ferrite and its dependence on the magnetic bias make ferrite a suitable choice to design a tunable CRLH structure [23]–[29]. However, to produce the LH response, simultaneous negative permittivity is also needed. In this article, the magnetized ferrite-blade waveguide is proposed as a tunable CRLH structure, where the rectangular waveguide operates below the cutoff frequency of the dominant mode. As an application of this tunable CRLH transmission line, a new LWA with the capability of continuous beam scanning is also designed.

This article is organized as follows: In Section II, the tunable CRLH response of the ferrite-blade waveguide is investigated. Based on the modal analysis, the dispersion diagram is obtained and validated by the numerical results. In Section III, by etching a longitudinal slot on the broad wall of this ferrite-blade waveguide, an LWA is designed. The equivalent circuit model and the beam scanning behavior of the proposed LWA are investigated in this section. Finally, in Section IV, a conclusion is given.

II. Ferrite-Blade Waveguide

This section investigates the proposed ferrite-blade waveguide given in Fig. 1. Based on the modal analysis, this structure is analyzed and its unbalanced CRLH response is shown. The calculated and simulated results show that the phase constant (β) of this structure can be tuned by both the magnetic field bias of the ferrite and the frequency. As shown

Manuscript received August 27, 2020; revised December 4, 2020 and January 8, 2021; accepted February 14, 2021. Date of publication February 22, 2021; date of current version March 18, 2021. Corresponding author: M. Mohammadi Shirkolaei (e-mail: m.mohammadi@ssau.ac.ir).

Color versions of one or more figures in this article are available at https://doi.org/10.1109/TMAG.2021.3060683.

Digital Object Identifier 10.1109/TMAG.2021.3060683

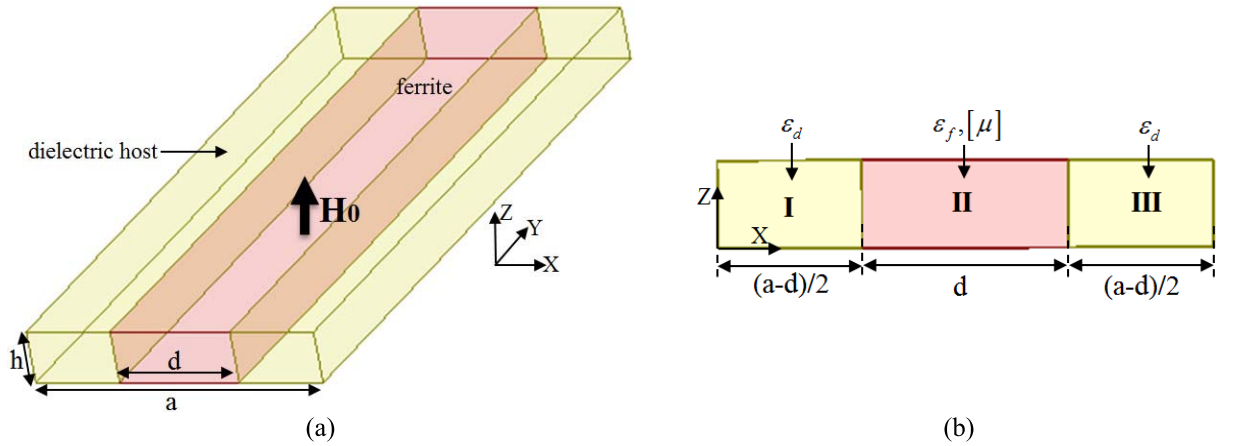

Fig. 1. Ferrite-blade waveguides. (a) 3-D. (b) Cross-sectional view.

in Section III, this structure is a good candidate to design a scannable LWA.

A. Unbalanced CRLH Response of the Ferrite-Blade Waveguide

Fig. 1 shows the ferrite-blade waveguide schematic, where the high permittivity dielectric host fills the other space of the waveguide. The magnetic bias of ferrite H_0 is applied normally to the guideline. Generally, the refractive index of this structure can be given as follows:

$$n = \begin{cases} +\sqrt{\mu_{\text{eff}}\varepsilon_{\text{eff}}} & \text{for : } \varepsilon_{\text{eff}} > 0,\ \mu_{\text{eff}} > 0 \text{ RH-region} \\ -\sqrt{\mu_{\text{eff}}\varepsilon_{\text{eff}}} & \text{for : } \varepsilon_{\text{eff}} < 0,\ \mu_{\text{eff}} < 0 \text{ LH-region} \end{cases} \tag{1}$$

where μ_{eff} and ε_{eff} are the effective permeability and permittivity of the ferrite-blade waveguide, respectively. In (1), μ_{eff} can be approximated as a function of the relative permeability of the host dielectric ($\mu_r = 1$) and the effective permeability of the normally magnetized ferrite (μ_e)

$$\mu_{\text{eff}} = \frac{d}{a}\mu_e + \frac{a-d}{a}\mu_r \tag{2}$$

where a and d are the width of waveguide and the ferrite-blade, respectively.

Based on [30], the effective permeability of the normally magnetized ferrite is obtained

$$\mu_e = \frac{\mu^2 - \mu_a^2}{\mu} \tag{3}$$

with

$$\mu = 1 + \frac{\omega_H\omega_M}{\omega_H^2 - \omega^2}, \quad \mu_a = \frac{\omega_M\omega}{\omega_H^2 - \omega^2},$$
$$\omega_H = \gamma H_0, \quad \omega_M = \gamma M_s \tag{4}$$

where M_s is the saturation magnetization, $\gamma = 2.8$ MHz/Oe is the gyromagnetic ratio, ω_H is the magnetic resonance frequency, ω_M is the saturation magnetic resonance frequency, and ω is the operating frequency. Note that, in all equations, the effect of the height of waveguide (h) is neglected, where h is much lower than a, and consequently, the electromagnetic fields have no variation in the z-direction.

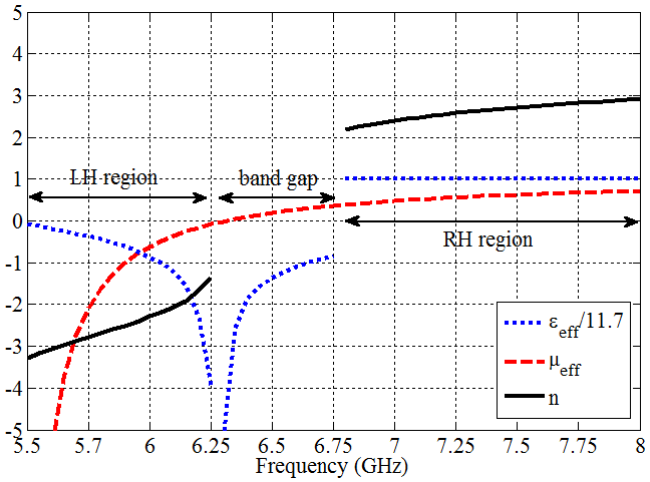

Fig. 2. Effective permeability in (2), the scaled effective permittivity in (5) (where $(d\varepsilon_f + (a-d)\varepsilon_d/a) = 11.7$) and the refractive index of ferrite-blade waveguide in (1). $4\pi Ms = 0.101$ T, $\varepsilon_f = 13.2$, and $\varepsilon_d = 9.2$, $a = 8$ mm, $d = 5$ mm, and $H_0 = 1500$ Oe.

If the operating frequency is less than the cutoff frequency of rectangular waveguide dominant mode, ε_{eff} (effective permittivity of the ferrite-blade waveguide) in (1) can be extracted based on the dielectric function of a no-loss plasma medium in the Drude model as follows [31]:

$$\varepsilon_{\text{eff}} = \frac{d\varepsilon_f + (a-d)\varepsilon_d}{a}\left(1 - \frac{\omega_c^2}{\omega^2}\right) \tag{5}$$

where ε_f and ε_d are the relative permittivity of the ferrite and the host dielectric, respectively. ω_c is the cutoff frequency of the rectangular waveguide [32]. As a result, negative effective permittivity causes a shunt inductor in the equivalent circuit of the rectangular wavelength.

According to (1), (2), and (5), the ferrite-blade waveguide has an LH response when both μ_{eff} and ε_{eff} are negative and has an RH response when both of μ_{eff} and ε_{eff} are positive. In addition, a non-propagation region separates the LH band from the RH band, where μ_{eff} is positive, and ε_{eff} is negative (see Fig. 2).

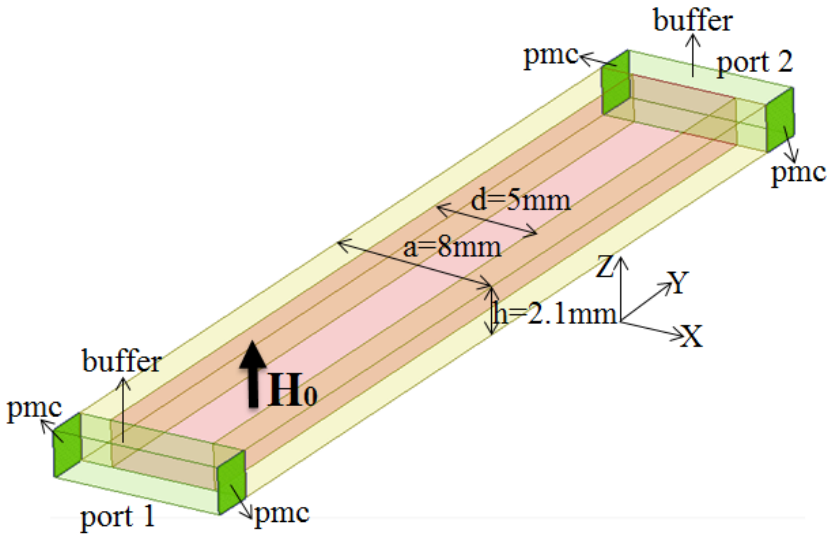

Fig. 3. Schematic of the ferrite-blade waveguide in HFSS software.

Fig. 2 shows the effective permeability in (2), the effective permittivity in (5), and the refractive index of the ferrite-blade waveguide in (1) with the design parameters given in the caption. As displayed in Fig. 2, the presented ferrite-blade waveguide has an LH property for the frequency below 6.3 GHz where both μ_{eff} and ε_{eff} are negative. There is a bandgap in the frequency range of 6.3–6.75 GHz, where an evanescent mode is excited due to positive μ_{eff} and negative ε_{eff} (waveguide below the cutoff frequency). Above the frequency of 6.8 GHz, the waveguide behaves in a typical manner in the RH region. In this region, both μ_{eff} and ε_{eff} are positive. As mentioned earlier, the ferrite-blade waveguide behaves as an unbalanced CRLH transmission line, where a bandgap separates the RH from the LH region.

B. Analysis of the Ferrite-Blade Waveguide

By assumption of $h \ll a$, the incident electromagnetic fields have no variation along the z-direction ($(\partial/\partial z) = 0$). In this case, the only TE_{n0} modes can be satisfied with the boundary conditions in the ferrite-blade waveguide structure in Fig. 1, where the ferrite blade is magnetized along the z-direction. Based on the equations presented in [25]–[28] and applying the boundary conditions, the dispersion relation for the ferrite-blade waveguide is summarized as follows:

$$2k_{xf}k_{xd}\cot(k_{xf}d)\cot\left(k_{xd}\frac{a-d}{2}\right)+\mu_e k_{xd}^2\cot^2\left(k_{xd}\frac{a-d}{2}\right)-\frac{k_{xf}^2+\zeta^2}{\mu_e}=0 \quad (6)$$

with

$$k_{xf}^2=\omega^2\varepsilon_0\mu_0\varepsilon_{\text{eff}}\mu_e-\beta^2 \quad (7)$$

$$k_{xd}^2=\omega^2\varepsilon_0\mu_0\varepsilon_{\text{eff}}-\beta^2 \quad (8)$$

$$\zeta=\frac{\mu_a\beta}{\mu} \quad (9)$$

where k_{xf} is the wavenumber of the region II, k_{xd} is the wavenumber of the region I and region III, and β is the phase constant along the waveguide (y-direction).

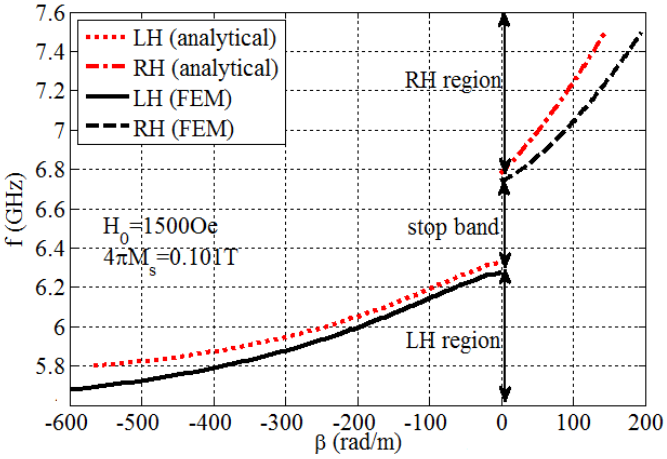

Fig. 4. Analytical and simulated dispersion relation of the ferrite-blade waveguide with the mentioned physical parameters in Fig. 2.

This dispersion relation will be plotted in Section II-C. As will be shown, the phase constant β in (6) can be tuned by the frequency and the magnetic field bias H_0.

C. Tunable CRLH Response of the Ferrite-Blade Waveguide

To verify the theoretical analysis and demonstrate the effects of magnetic field bias on the dispersion diagram, the presented ferrite-blade waveguide is simulated by the commercial software HFSS based on the finite-element method (FEM). Fig. 3 shows the schematic of this structure in HFSS. Since it is impossible to connect an excited port to anisotropic material in HFSS, the two short length dielectric-filled parallel-plate waveguides (PPWs) with perfect magnetic conductor (PMC) at narrow wall, as buffers, have been placed at both ends of the structure where the relative permittivity of the buffers is similar to the host dielectric.

Fig. 4 shows the calculated dispersion diagram obtained from (6) and the simulated results obtained by HFSS. Note that, the simulated dispersion diagram only relates to the

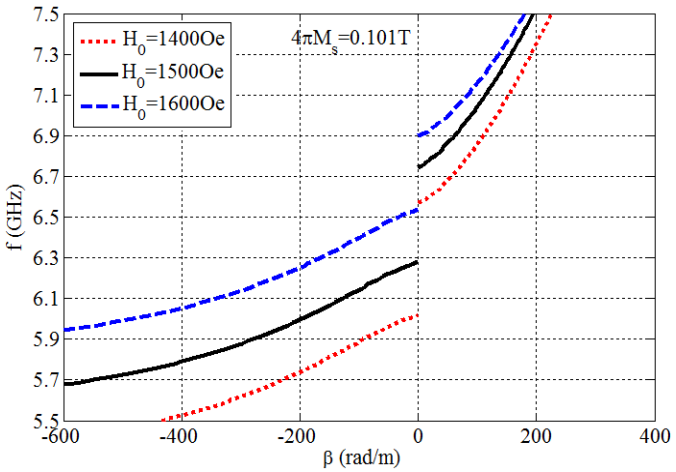

Fig. 5. Dispersion diagram of the ferrite-blade waveguide for several magnetic field biases with the mentioned physical parameters in Fig. 2.

blade-ferrite waveguide and the effect of the buffers has been eliminated. Based on the theoretical and simulated results in Fig. 4, the proposed structure has an unbalanced CRLH response. Compared to Fig. 2, this bandgap is matched to the frequency range where the effective permeability and permittivity of the ferrite-blade waveguide are positive and negative, respectively.

Fig. 5 shows the dispersion diagram of the ferrite-blade waveguide for the several magnetic field biases (H_0 = 1400, 1500, and 1600 Oe). These results prove the tunable unbalanced CRLH response of the proposed structure, where, increasing H_0 will lead to a shift in both LH and RH bands to higher frequencies. As shown in Section III, this structure can be used to design a new backward-to-forward beam-scanning LWA antenna.

III. LWA Based on the Ferrite-Blade Waveguide

Now, we present an LWA consisting of a longitudinal slot built on the upper wall of the ferrite-blade waveguide. Based on the transverse resonance method (TRM), presented in [32], the equivalent circuit model of this LWA is extracted, and the dispersion relation is calculated. As will be shown in the results, the radiation beam of this antenna can be continuously scanned from the backward (−) to forward (+) angles.

A. Equivalent Circuit Model and Dispersion Relation of the LWA

Fig. 6(a) shows the slotted ferrite-blade waveguide. Generally, the rectangular waveguide with a longitudinal radiation slot on the upper wall is equivalent to an E-plane T-junction that is consisted of the three arms, named A, B, and C in Fig. 6 [27], [33]. By using the TRM, the equivalent circuit model of this junction is obtained and shown in Fig. 6(b), where each part is explained as follows:

As shown in Fig. 6(b), arm A consists of two parts. The first part is a short-ended dielectric-filled transmission line with the length of $(a-d)/2$, characteristic admittance of Y_{cd}, and the wavenumber of k_{xd}. The second part is a normally magnetized ferrite-filled transmission line with the length of $d/2+x_{ofs}$ and the wavenumber of k_{xf}. Arm C is similar to arm A but the length of its ferrite part (second part) is $d/2-x_{ofs}$. The characteristic admittance Y_{cd} of the dielectric part, as a dielectric-loaded rectangular waveguide, can be calculated by [32]

$$Y_{cd}=\frac{k_{xd}}{\omega\mu_0} \tag{10}$$

where k_{xd} is given in (8).

The ferrite part of arms A and C, as a ferrite-loaded rectangular waveguide, is modeled by the two admittances, the isotropic (Y_c), and anisotropic admittance (Y_{an}) of the ferrite [34]. These admittances are described in the term of the ferrite parameters as [35]

$$Y_c=\frac{k_{xf}}{\omega\mu_0\mu_e} \tag{11}$$

$$Y_{\text{an}}=j\frac{\mu_a}{\mu}\frac{\beta}{\omega\mu_0\mu_e} \tag{12}$$

where μ_e, μ, μ_a, and k_{xf} are given in (3), (4), and (7), respectively.

The arm B in Fig. 6 can be considered as an open-ended hollow PPW with the length of t, the distance between plate w_s, characteristic admittance of Y_0, and the wavenumber of k_{t0} that radiates to the upper free space of the waveguide. The admittance of the radiating slot ($Y_{LB}=G+jB$) with unlimited length and width of w_s is given by [36]

$$\frac{G}{Y_0}=\frac{\pi w_s}{2\lambda},\quad w_s\ll\lambda \tag{13}$$

$$\frac{B}{Y_0}=\frac{w_s}{\lambda}\ln\left(\frac{2e\lambda}{\delta w_s}\right),\quad w_s\ll\lambda \tag{14}$$

where $e=2.718$, $\delta=1.781$, and λ is the wavelength of the PPW. Since our operating frequency is within the C-band and the cut off frequency of the first PPW mode according to the slot width ($w_s=1$ mm) is equal to

$$f_c=\frac{1}{2w_s\sqrt{\varepsilon_0\mu_0}}=150.15\ \text{GHz}. \tag{15}$$

Therefore, the propagation mode in the PPW can be considered the TEM mode. According to this, the wavelength expressed in (13) and (14) is considered as follows:

$$\lambda=\frac{1}{f\sqrt{\varepsilon_0\mu_0}}. \tag{16}$$

The two parallel susceptances of B_a and the series susceptance of B_b are used to model the E-plane waveguide T-junction in Fig. 6 [33]

$$\frac{B_a}{Y_c}=\frac{\frac{h}{\lambda_g}\left(\frac{\pi w_s}{4h}\right)^2}{1+\frac{1}{6}\left(\frac{\pi w_s}{4h}\right)^2\left\{\left(\frac{h}{w_s}\right)^2+\frac{1}{2}\right\}},\quad w_s,\quad h\ll\lambda_g \tag{17}$$

$$\frac{B_b}{Y_c}=\frac{4h}{\lambda_g}\left[\ln\frac{2\sqrt{2}\,h}{\pi}+\left(\frac{h}{\lambda_g}\right)^2\right],\quad h\ll\lambda_g \tag{18}$$

where

$$\lambda_g=\frac{2\pi}{\beta},\quad \beta=\sqrt{\omega^2\varepsilon_0\varepsilon_{\text{eff}}\mu_0\mu_e-k_{xf}^2}. \tag{19}$$

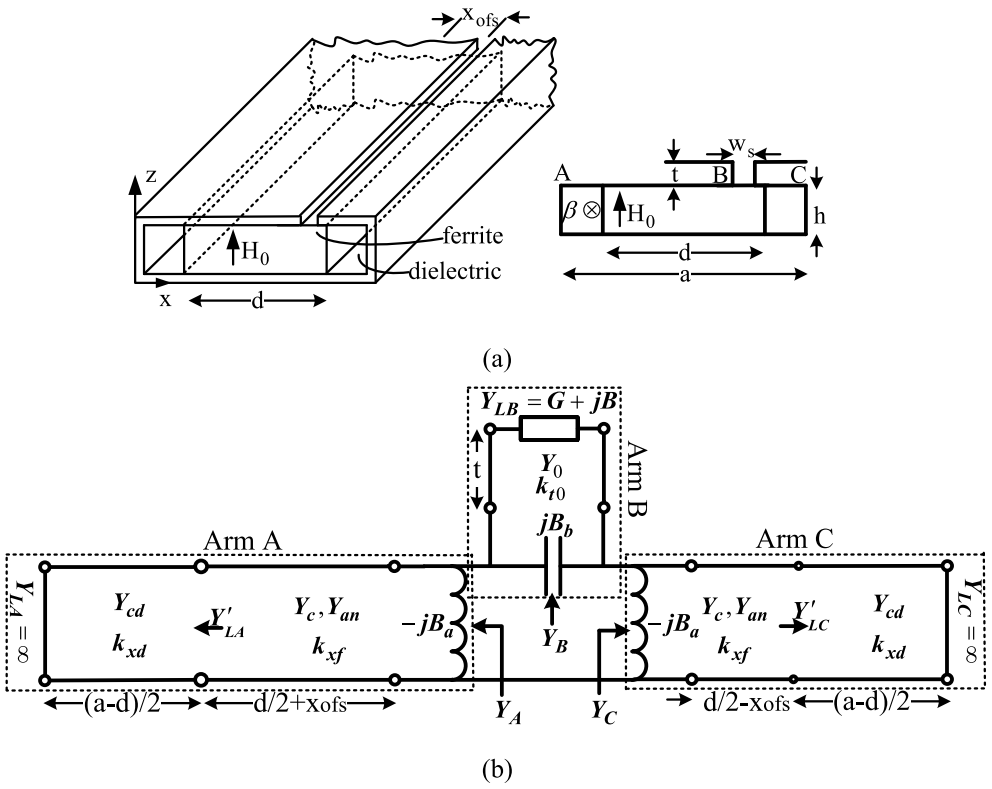

Fig. 6. (a) Slotted ferrite-blade waveguide and (b) equivalent circuit model based on TRM.

Compared to the equivalent circuit model of a typical CRLH line, B_a and B_b in Fig. 6(b) can play the role of parallel inductor (L_L) and series capacitor (C_L), respectively [27].

As shown in Fig. 6(b), Y_A, Y_B, and Y_C introduce the input admittance of the arms A, B, and C. Based on the TRM, these admittances must satisfy the condition

$$Y_A + Y_B + Y_C = 0 \tag{20}$$

where Y_A, Y_B, and Y_C are calculated as

$$Y_A = -jB_a + Y_{\text{an}} + j\frac{Y'_{LA} + jY_c \tan[k_{xf}(d/2 + x_{ofs})]}{Y_c + jY'_{LA}\tan[k_{xf}(d/2 + x_{ofs})]} \tag{21}$$

$$Y_C = -jB_a + Y_{\text{an}} + j\frac{Y'_{LC} + jY_c \tan[k_{xf}(d/2 - x_{ofs})]}{Y_c + jY'_{LC}\tan[k_{xf}(d/2 - x_{ofs})]} \tag{22}$$

$$Y_B = jB_b + Y_0\frac{Y_{LB} + jY_0 \tan(k_{t0}t)}{Y_0 + jY_{LB}\tan(k_{t0}t)}. \tag{23}$$

As shown in Fig. 6(b), Y'_{LA} and Y'_{LC} present the input admittance of the dielectric part of the arms A and C, respectively

$$Y'_{LA} = Y'_{LC} = jY_{cd}\cot\left(k_{xd}\frac{a-d}{2}\right). \tag{24}$$

The length of arm B is equal to the waveguide thickness (t) and much lower than the wavelength λ. Therefore, Y_B can be approximated by

$$Y_B = jB_b + Y_{LB} = jB_b + G + jB. \tag{25}$$

By substituting (21), (22), and (25) into (20), the dispersion relation can be calculated

$$-j2B_a + 2Y_{\text{an}} + j\frac{Y'_{LA} + jY_c \tan[k_{xf}(d/2 + x_{ofs})]}{Y_c + jY'_{LA}\tan[k_{xf}(d/2 + x_{ofs})]} + j\frac{Y'_{LC} + jY_c \tan[k_{xf}(d/2 - x_{ofs})]}{Y_c + jY'_{LC}\tan[k_{xf}(d/2 - x_{ofs})]} + jB_b + G + jB = 0. \tag{26}$$

However, there is no analytical method for solving this relation. But, some methods such as Newton's method can be used to plot the dispersion diagram ($\beta - f$).

Note that, the permeability of μ_e in (3), the wavenumber k_{xf} in (7) and consequently, the calculated β from (26) are depending on magnetic bias field H_0.

To validate the analytical dispersion relation obtained in (26), the slotted ferrite-blade waveguide is simulated by HFSS based on FEM. The schematic of the proposed structure is shown in Fig. 7, where the two buffers are also used at both ends. The ferrite characteristics and the geometrical parameters are given in Table I. Fig. 8 presents the dispersion diagram of the slotted ferrite-blade waveguide obtained from (26) and the simulated results obtained by HFSS. It can be seen an approximately good agreement between the analytical and simulation results. Furthermore, the phase constant in Fig. 8 can be varied from the negative to the positive values without any frequency bandgap. This balanced CRLH behavior is due to the slot inductive effect on the ferrite-blade waveguide response in Section II.

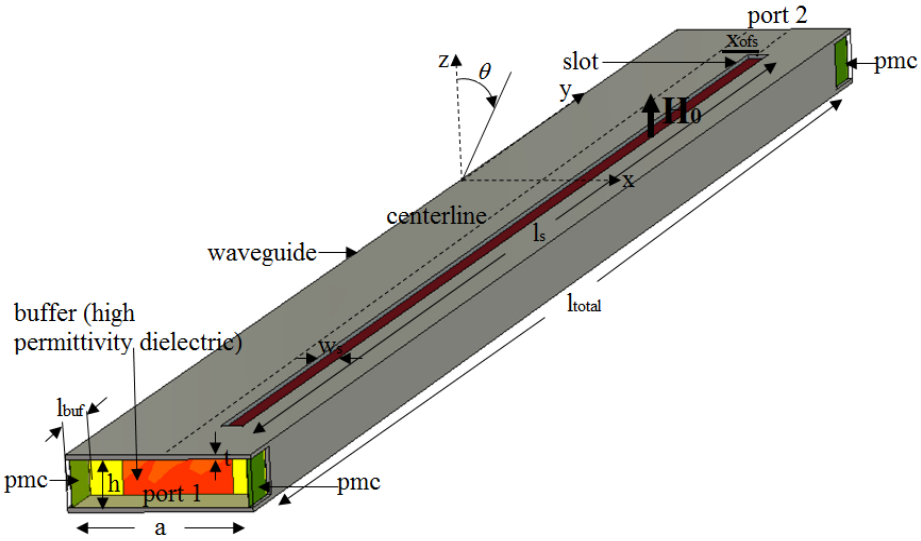

Fig. 7. Schematic model of the ferrite-blade waveguide with a longitudinal slot in HFSS.

TABLE I
PARAMETERS OF THE PROPOSED LONGITUDINAL SLOT LWA

$4\pi M_s$	0.101T	w_s	1mm
ε_f	13.2	l_s	92.5mm
ε_d	9.2	x_{ofs}	1.5mm
A	8mm	t	0.1mm
H	2.1mm	l_{total}	100mm
D	5mm	l_{buf}	3mm

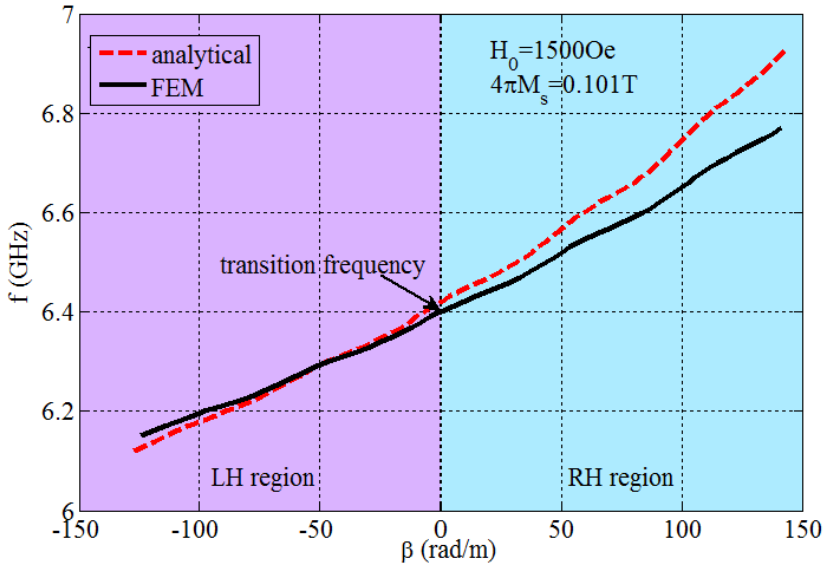

Fig. 8. Calculated dispersion diagram obtained from (26) and the simulated dispersion diagram of the ferrite-blade waveguide with a longitudinal slot.

To show the balanced CRLH behavior of the proposed LWA in Fig. 7, the electrical field along the proposed LWA at different frequencies for two different excitation phases of the input port ($\varphi = 0°$ and 80°) is plotted in Fig. 9. As shown in Fig. 9(a), at the frequency of 6.2 GHz in the LH region where the phase constant in Fig. 8 is negative, the group and phase velocities are forward and backward, respectively. In the frequency of 6.4 GHz, the transition frequency between the LH and RH regions in Fig. 8, the phase constant is 0, and consequently, the wavelength is infinite. As shown in Fig. 9(b), at the transition frequency, the maximum value of the electric field does not oscillate along with the waveguide. Based on the dispersion diagram in Fig. 8, at the transition frequency, the group velocity is not 0, and there is a propagating wave. Finally, Fig. 9(c) shows the phase and the group velocity at the frequency of 6.7 GHz in the RH region of Fig. 8, where both

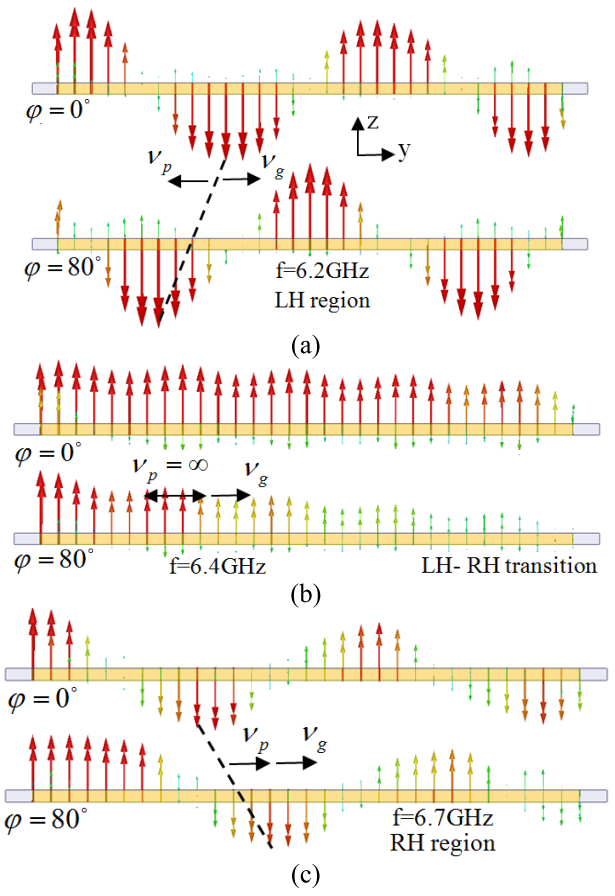

Fig. 9. Electrical field distribution along the longitudinal slot on the ferrite blade waveguide under $H_0 = 1500$ Oe. (a) LH region, (b) transition frequency, and (c) RH region. (The source has been located on the left.)

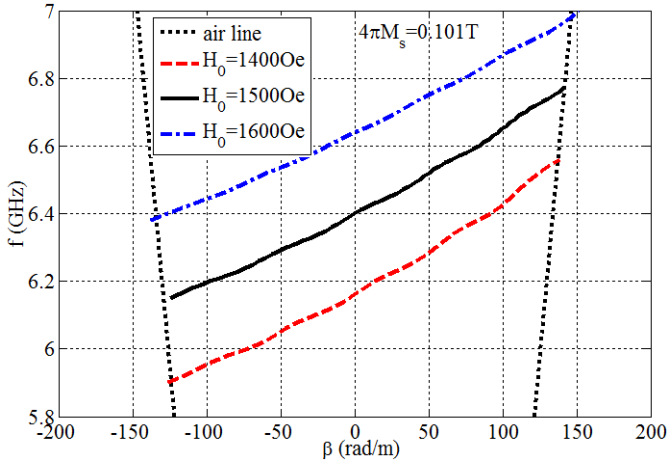

Fig. 10. Dispersion diagram of the longitudinal slot LWA based on the ferrite blade waveguide for the different magnetic field biases (air lines: $\beta = \pm k_0$).

velocities are in the forward direction. This balanced CRLH behavior validates the capability of the proposed LWA in producing a continuous backward-to-forward beam-scanning.

B. Scanning Ability of the LWA

Fig. 10 shows the dispersion diagram of the presented LWA in Fig. 8 under several magnetic field biases. As shown

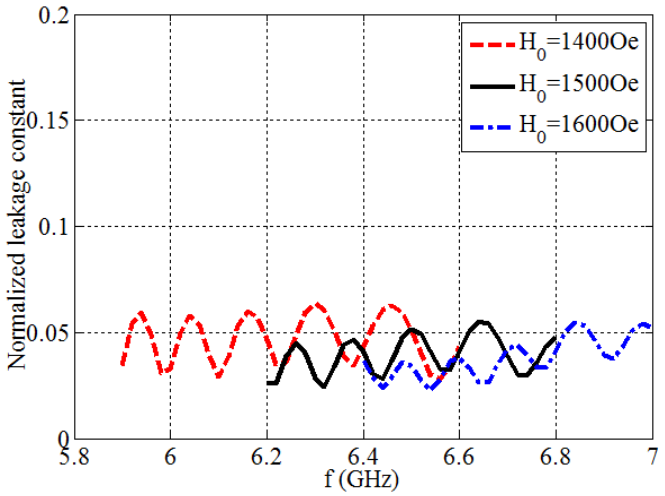

Fig. 11. Normalized attenuation (leakage) constant (α/k_0) of the longitudinal slot LWA based on the ferrite blade waveguide for different magnetic field biases.

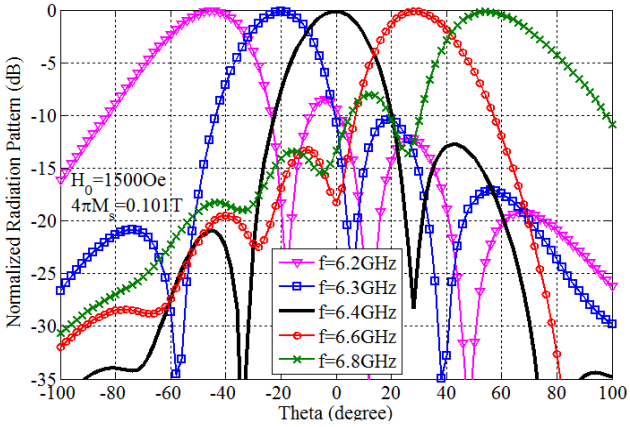

Fig. 12. Radiation pattern of the proposed LWA in different frequencies at $H_0 = 1500$ Oe.

in Fig. 8, increasing H_0 will lead to a shift in the LH and RH regions to higher frequencies. The results shown in Fig. 10 validate the tunable balanced CRLH response of this structure. Fig. 11 shows the normalized leakage constant of the longitudinal slot LWA based on the ferrite blade waveguide for different magnetic field biases obtained using (27). As shown in Fig. 11, the normalized leakage constant is smaller than 0.06 for each bias dc. As a result, this amount of leakage constant is proper to use this structure as a high gain antenna [37]

$$\frac{\alpha}{k_0} = -\frac{\ln|S_{21}|}{l_{\text{total}}}. \tag{27}$$

In a typical LWA, the wave is leaked out when the absolute value of phase constant β is lower than the free space wavenumber k_0 [10]. Fig. 10 shows the proposed slotted ferrite-blade waveguide has a radiation cone where $-k_0 < \beta < k_0$. As the main advantage, β can be continuously varied from the negative values to positive by changing in the frequency or the magnetic bias, independently. It means; the proposed structure is operated as an LWA with continuous beam scanning from backfire to endfire, where the main beam

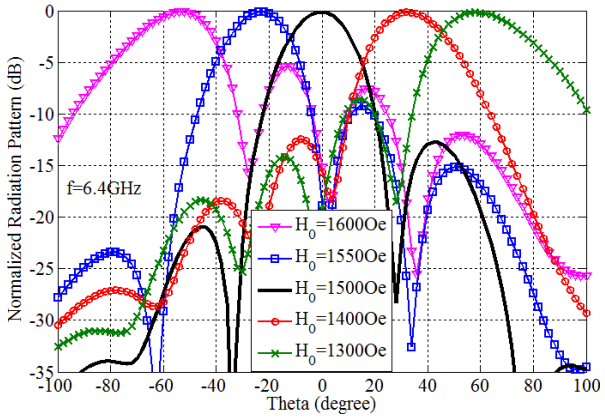

Fig. 13. Radiation pattern of the proposed LWA at a frequency of 6.4 GHz for different magnetic field biases.

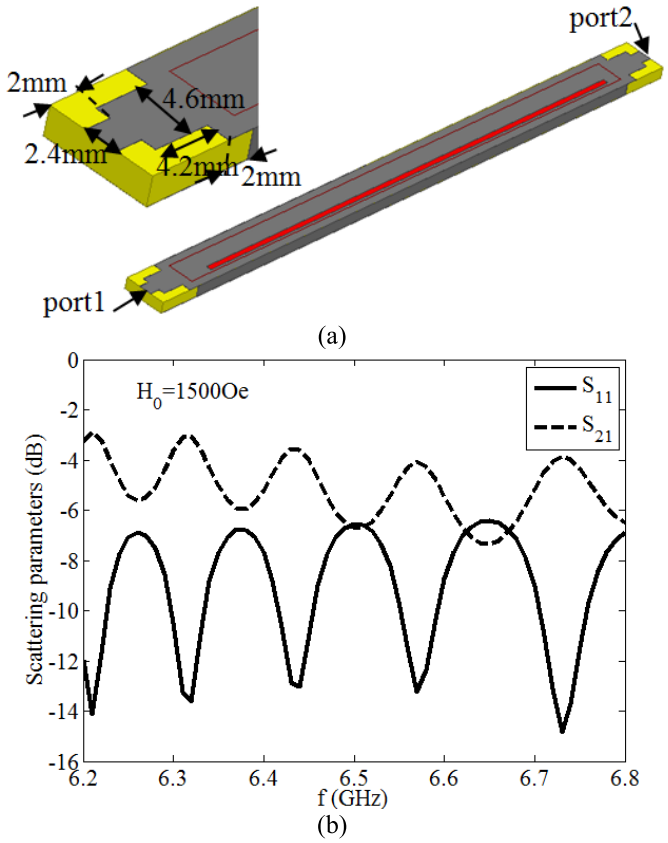

Fig. 14. (a) Overall view and detailed view of the feed line section of the proposed LWA. (b) Return loss (S_{11}) and transmission loss (S_{21}) of the proposed LWA.

direction is given by [26], [27]

$$\theta_{MB}(\omega, H_0) = \sin^{-1}\left[\frac{\beta(\omega, H_0)}{k_0}\right]. \tag{28}$$

As another advantage, the proposed LWA has a uniform structure compared to previous cellular CRLH structures.

Fig. 12 shows the simulated radiation patterns of the presented LWA under $H_0 = 1500$ Oe at some frequencies. It is seen in Fig. 12 that the direction of the main beam changed from negative to positive that confirms the multi-frequency continuous beam scanning capacity of the proposed antenna

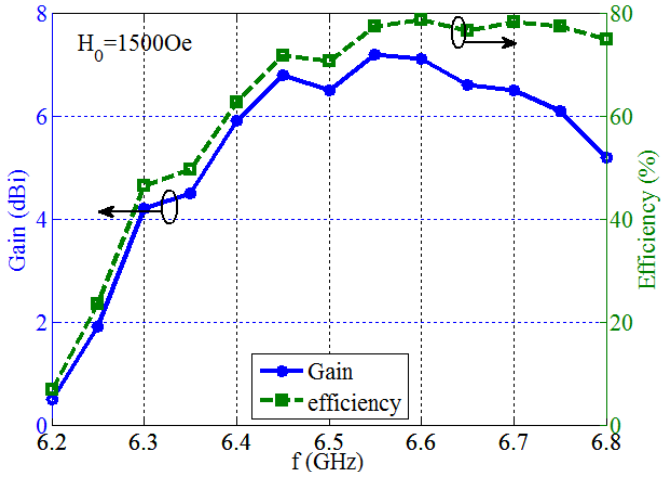

Fig. 15. Gain and efficiency versus frequency for the proposed LWA.

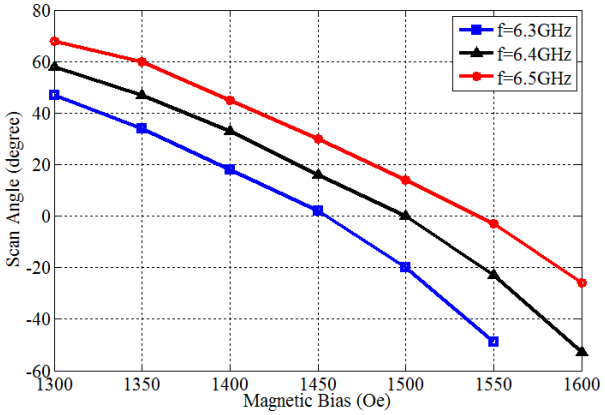

Fig. 16. Main beam angle of the LWA versus the magnetic field bias for different frequencies.

for the fixed magnetic field bias. Furthermore, the simulated radiation patterns at the frequency of 6.4 GHz for different magnetic biases are shown in Fig. 13. As shown in Fig. 13, the scan angle changes from negative values to positive ones at a fixed frequency. These results confirm that the proposed LWA has a scannable radiation beam, by a change in the operation frequency or the magnetic field bias, independently.

Fig. 14(a) shows the detailed configuration of the prototype, including the feed line section. The dimensions of the antenna structure are identical to that shown in Fig. 7 and Table I. The return loss and transmission loss for the antenna prototype are presented in Fig. 14(b). Fig. 15 illustrates the gain and efficiency versus frequency for the proposed LWA at $H_0 = 1500$ Oe. The peak gain and efficiency of the proposed antenna are 7.1 dBi and 78.5% at 6.6 GHz, respectively.

Fig. 16 presents the variation of the main beam angle of the LWA versus the magnetic bias field. For example, the scanning range at the fixed frequency of 6.4 GHz is $-57°$ to $+59°$ that is wider than the other previous LWAs [26], [27], and [38]. In addition, as shown in Fig. 17, the cross-polarization (XP) levels of the proposed LWA are less than -36 dB. Compared to some other works such as [26], [27], and [39], the XP levels have been significantly decreased.

TABLE II
PROPOSED ANTENNA PERFORMANCE COMPARISON

	[25]	[24]	[38]	This Work
Freq. (GHz)	5.7-6.3 @H0=1910Oe	LH:9.5-10.3 RH:11.7-12.8 @H0=800 Oe	10 @H0=1033Oe	**6.2-6.8 @H0=1500Oe**
Antenna length	2λ0 @5.9GHz	3λ0 @11 GHz	4.7λ0 @10 GHz	**1.97λ0 @ 6.4GHz**
Radiation at $\theta = 0^\circ$	Yes	No	No	**Yes**
Scan range	-20° to 50°	-38° to -12° 10° to 37°	-70° to -30° 10° to 43°	**-53° to 58°**
Maximum Gain(dBi)	4.9	Not reported	Not reported	**7.2**
Cross-polarization(dB)	Not reported	Not reported	Not reported	**-36**

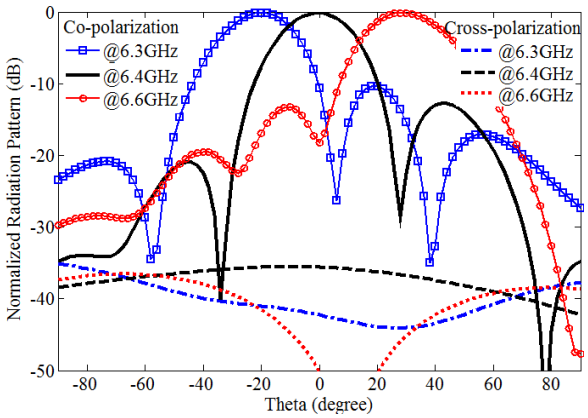

Fig. 17. Co- and cross-polarization for the LWA in the several frequencies at $H_0 = 1500$ Oe.

Table II lists the comparison of the performance of the proposed LWA antenna with other related works in the literature.

IV. CONCLUSION

A new CRLH structure that consists of a ferrite-blade in the rectangular waveguide is proposed. The main idea in this work is adding the inherent negative permeability of biased ferrite to the negative permittivity behavior of the below cutoff rectangular waveguide at the common frequency band. Based on the calculated and simulated results, this structure shows the tunable CRLH response that can be used as an LWA. The radiation beam of this LWA can be scanned by using the operation frequency or the ferrite magnetic bias, independently. For example, it can be continuously scanned from $+59°$ to $-57°$ by varying the magnetic bias of the ferrite from 1400 to 1600 Oe, where the operation frequency is 6.4 GHz. Compared to the previous LWAs, the proposed antenna has a backward-to-forward beam-scanning capability without using any chip components such as MEMS, varactor, and p-i-n diode.

REFERENCES

[1] S. M. M. Moshiri, M. Khodadadi, and N. Nozhat, "Compact and wideband bandpass filters with analysis of the CRLH-TL characteristics based on stepped impedance resonator," *AEU-Int. J. Electron. Commun.*, vol. 108, pp. 96–106, Aug. 2019.

[2] V. R. Nuthakki and S. K. Dhamodharan, "Bandwidth enhancement of ZOR antenna by loading novel via-less CRLH-TL unit cells," *AEU-Int. J. Electron. Commun.*, vol. 83, pp. 501–511, Jan. 2018.

[3] M. A. Abdalla and Z. Hu, "Tunable characteristics of ferrite composite right/left handed coplanar waveguide coupled line coupler—Measurement and experimental verification," *AEU-Int. J. Electron. Commun.*, vol. 96, pp. 113–121, Nov. 2018.

[4] M. Alibakhshi-Kenari and M. Naser-Moghadasi, "Novel UWB miniaturized integrated antenna based on CRLH metamaterial transmission lines," *AEU-Int. J. Electron. Commun.*, vol. 69, no. 8, pp. 1143–1149, Aug. 2015.

[5] T. Tsutaoka, T. Kasagi, S. Yamamoto, and K. Hatakeyama, "Double negative electromagnetic property of granular composite materials in the microwave range," *J. Magn. Magn. Mater.*, vol. 383, pp. 139–143, Jun. 2015.

[6] Z. Mazani, A. Abdipour, and K. Afrooz, "Matrix power amplifier with open-circuit composite right/left-handed transmission line," *IEEE Microw. Wireless Compon. Lett.*, vol. 29, no. 3, pp. 231–233, Mar. 2019.

[7] Z. Mazani, A. Abdipour, and K. Afrooz, "Active dual-band power divider and active quad-plexer based on traveling wave amplification and D-CRLH transmission line," *IEEE Trans. Circuits Syst. II, Exp. Briefs*, vol. 67, no. 3, pp. 480–484, Mar. 2020.

[8] D. K. Karmokar, Y. J. Guo, S.-L. Chen, and T. S. Bird, "Composite right/left-handed leaky-wave antennas for wide-angle beam scanning with flexibly chosen frequency range," *IEEE Trans. Antennas Propag.*, vol. 68, no. 1, pp. 100–110, Jan. 2020.

[9] Y. Kushiyama, T. Arima, and T. Uno, "Differential-type CRLH leaky-wave antenna using stepped impedance resonators," *IEEE Antennas Wireless Propag. Lett.*, vol. 15, pp. 321–324, 2016.

[10] M. M. Sabahi, A. A. Heidari, and M. Movahhedi, "A compact CRLH circularly polarized leaky-wave antenna based on substrate-integrated waveguide," *IEEE Trans. Antennas Propag.*, vol. 66, no. 9, pp. 4407–4414, Sep. 2018.

[11] A. Sarkar, A. Sharma, A. Biswas, and M. J. Akhtar, "EMSIW-based compact high gain wide full space scanning LWA with improved broadside radiation profile," *IEEE Trans. Antennas Propag.*, vol. 67, no. 8, pp. 5652–5657, Aug. 2019.

[12] Q. Yang, X. Zhao, and Y. Zhang, "Design of CRLH leaky-wave antenna with low sidelobe level," *IEEE Access*, vol. 7, pp. 178224–178234, 2019.

[13] D. K. Karmokar, S.-L. Chen, T. S. Bird, and Y. J. Guo, "Single-layer multi-via loaded CRLH leaky-wave antennas for wide-angle beam scanning with consistent gain," *IEEE Antennas Wireless Propag. Lett.*, vol. 18, no. 2, pp. 313–317, Feb. 2019.

[14] M. Alibakhshikenari *et al.*, "Beam-scanning leaky-wave antenna based on CRLH-metamaterial for millimetre-wave applications," *IET Microw., Antennas Propag.*, vol. 13, no. 8, pp. 1129–1133, Jul. 2019.

[15] A. Sarkar, M. Adhikary, A. Sharma, A. Biswas, M. J. Akhtar, and Z. Hu, "Composite right/left-handed based compact and high gain leaky-wave antenna using complementary spiral resonator on HMSIW for Ku band applications," *IET Microw., Antennas Propag.*, vol. 12, no. 8, pp. 1310–1315, Jul. 2018.

[16] Y. Dong and T. Itoh, "Composite right/left-handed substrate integrated waveguide and half mode substrate integrated waveguide leaky-wave structures," *IEEE Trans. Antennas Propag.*, vol. 59, no. 3, pp. 767–775, Mar. 2011.

[17] Q. Yang, X. Zhao, and Y. Zhang, "Composite right/left-handed ridge substrate integrated waveguide slot array antennas," *IEEE Trans. Antennas Propag.*, vol. 62, no. 4, pp. 2311–2316, Apr. 2014.

[18] G. Zamora, S. Zuffanelli, F. Paredes, F. J. Herraiz-Martinez, F. Martin, and J. Bonache, "Fundamental-mode leaky-wave antenna (LWA) using slotline and split-ring-resonator (SRR)-based metamaterials," *IEEE Antennas Wireless Propag. Lett.*, vol. 12, pp. 1424–1427, 2013.

[19] N. Nasimuddin, Z. N. Chen, and X. Qing, "Substrate integrated metamaterial-based leaky-wave antenna with improved boresight radiation bandwidth," *IEEE Trans. Antennas Propag.*, vol. 61, no. 7, pp. 3451–3457, Jul. 2013.

[20] N. Nasimuddin, Z. N. Chen, and X. Qing, "Multilayered composite right/left-handed leaky-wave antenna with consistent gain," *IEEE Trans. Antennas Propag.*, vol. 60, no. 11, pp. 5056–5062, Nov. 2012.

[21] S. Lim, C. Caloz, and T. Itoh, "Metamaterial-based electronically controlled transmission-line structure as a novel leaky-wave antenna with tunable radiation angle and beamwidth," *IEEE Trans. Microw. Theory Techn.*, vol. 53, no. 12, pp. 161–173, Dec. 2005.

[22] S.-L. Chen, D. K. Karmokar, Z. Li, P.-Y. Qin, R. W. Ziolkowski, and Y. J. Guo, "Continuous beam scanning at a fixed frequency with a composite right-/left-handed leaky-wave antenna operating over a wide frequency band," *IEEE Trans. Antennas Propag.*, vol. 67, no. 12, pp. 7272–7284, Dec. 2019.

[23] J. Ghalibafan, N. Komjani, and B. Rejaei, "Tunable left-handed characteristics of ferrite rectangular waveguide periodically loaded with complementary split-ring resonators," *IEEE Trans. Magn.*, vol. 49, no. 8, pp. 4780–4784, Aug. 2013.

[24] E. K. Berneti and J. Ghalibafan, "Tunable ferrite-based metamaterial structure and its application to a leaky-wave antenna," *J. Magn. Magn. Mater.*, vol. 456, pp. 223–227, Jun. 2018.

[25] T. Kodera and C. Caloz, "Uniform ferrite-loaded open waveguide structure with CRLH response and its application to a novel backfire-to-endfire leaky-wave antenna," *IEEE Trans. Microw. Theory Techn.*, vol. 57, no. 4, pp. 784–795, Apr. 2009.

[26] M. Mohammadi, F. H. Kashani, and J. Ghalibafan, "A partially ferrite-filled rectangular waveguide with CRLH response and its application to a magnetically scannable antenna," *J. Magn. Magn. Mater.*, vol. 491, Dec. 2019, Art. no. 165551, doi: 10.1016/j.jmmm.2019.

[27] M. Mohammadi, F. H. Kashani, and J. Ghalibafan, "Backfire-to-endfire scanning capability of a balanced metamaterial structure based on slotted ferrite-filled waveguide," *Waves Random Complex Media*, pp. 1–15, Aug. 2019, doi: 10.1080/17455030.2019.1654148.

[28] M. M. Shirkolaei and J. Ghalibafan, "Unbalanced CRLH behavior of ferrite-loaded waveguide operated below cutoff frequency," *Waves Random Complex Media*, pp. 1–16, Aug. 2020, doi: 10.1080/17455030.2020.1800133.

[29] M. M. Shirkolaei and M. Aslinezhad, "Substrate integrated waveguide filter based on the magnetized ferrite with tunable capability," *Microw. Opt. Technol. Lett.*, pp. 1–6, Nov. 2020, doi: 10.1002/mop.32722.

[30] S.-C. Su, H.-Y. Yao, and T.-H. Chang, "Characterization of ferrites using a fully loaded waveguide system," *J. Magn. Magn. Mater.*, vol. 505, Jul. 2020, Art. no. 166712.

[31] A. Dechant and M. Okoniewski, "Broadband double negative material from ferrite-loaded metallic waveguides," *Electron. Lett.*, vol. 42, no. 1, pp. 4–7, Jan. 2006.

[32] C. A. Balanis, *Advanced Engineering Electromagnetics*, 2nd ed. New York, NY, USA: Wiley, 2012.

[33] J. A. G. Malherbe and J. Joubert, "Radiation properties of a long slot in the broad wall of a waveguide," *Electron. Lett.*, vol. 34, no. 6, pp. 568–570, Mar. 1998.

[34] C. Di Nallo, F. Frezza, A. Galli, and G. Gerosa, "A convenient transmission-line formulation for wave propagation in typical ferrite structures," *IEEE Trans. Magn.*, vol. 32, no. 4, pp. 3228–3236, Jul. 1996.

[35] T. Kodera and C. Caloz, "Leakage control in the CRLH uniform ferrite-loaded open waveguide leaky-wave antenna using a transversally extending evanescent waveguide structure," in *Proc. Asia–Pacific Microw. Conf.*, Yokohama, Japan, Dec. 2010, pp. 869–872.

[36] N. Marcuvitz, *Waveguide Handbook*. New York, NY, USA: McGraw-Hill, 1951.

[37] C. Caloz and T. Itoh, *Electromagnetic Metamaterials: Transmission Line Theory and Microwave Applications*. Hoboken, NJ, USA: Wiley, 2005.

[38] K. C. Hwang and H. J. Eom, "Radiation from a ferrite-filled rectangular waveguide with multiple slits," *IEEE Microw. Wireless Compon. Lett.*, vol. 15, no. 5, pp. 345–347, May 2005.

[39] H. Zhang, Y. Jiao, G. Zhao, and C. Zhang, "CRLH-SIW-based leaky wave antenna with low cross-polarisation for Ku-band applications," *Electron. Lett.*, vol. 52, no. 17, pp. 1426–1428, Aug. 2016.